PAPER

ZIF-95 as a filler for enhanced gas separation performance of polysulfone membrane†

Sanaullah Shafiq, [a] Bassem A. Al-Maythalony, [bc] Muhammad Usman, [d] Mohammad Saleh Ba-Shammakh[a] and Abdallah A. Al-Shammari *[a]

Metal–organic frameworks (MOFs) are found to be promising porous crystalline materials for application in gas separation. Considering that mixed matrix membranes usually increase the gas separation performance of a polymer by increasing selectivity, permeability, or both (*i.e.*, perm-selectivity), the zeolitic imidazole framework-95 (ZIF-95) MOF was dispersed for the first time in polysulfone (PSF) polymer to form mixed matrix membranes (MMMs), namely, ZIF-95/PSF. The fabricated ZIF-95/PSF membranes were examined for the separation of various gases. The characterization of solvothermally synthesized ZIF-95 was carried out using different analyses such as powder X-ray diffraction (PXRD), scanning electron microscopy (SEM), thermogravimetric analysis (TGA), porosity measurements, *etc.* ZIF-95 was mixed with PSF at 8%, 16%, 24%, and 32% weight percent to form different loading MMMs. SEM analysis of membranes revealed good compatibility/adhesion between the MOF and polymer. The permeability of He, H_2, O_2, CO_2, N_2, and CH_4 were measured for the pure and composite membranes. The ideal selectivity of different gas pairs were calculated and compared with reported mixed matrix membranes. The maximum increases in permeabilities were observed in 32% loaded membrane; nevertheless, these performance/permeability increases were at the expense of a slight decrease of selectivity. In the optimally loaded membrane (*i.e.*, 24 wt% loaded membrane), the permeability of H_2, O_2, and CO_2 increased by 80.2%, 78.0%, and 67.2%, respectively, as compared to the pure membrane. Moreover, the selectivity of H_2/CH_4, O_2/N_2, and H_2/CO_2 gas pairs also increased by 16%, 15%, and 8% in the 24% loaded membrane, respectively.

1 Introduction

Membrane technology is considered a promising gas separation technique due to its continuous, simple, and environmental-friendly operation.[1–4] Conventionally, the separation and purification of gases are done by absorption, adsorption, or cryogenic processes.[5] Adsorption/absorption based separation requires continuous regeneration of adsorbent/absorbent, which resultantly increases the operational and capital cost of separation. Similarly, the cryogenic separation of gases is also energy-intensive because it requires extremely high pressure and cryogenic temperature. The challenges faced by prevailing technologies can easily be overcome by membrane-based gas separation technology. The main industrial applications of membrane gas separation are natural gas sweetening (CO_2/CH_4), carbon capture (CO_2/N_2), hydrogen recovery (H_2/CH_4), syngas ratio adjustment (H_2/CO_2), nitrogen removal (N_2/CH_4), oxygen enrichment (O_2/N_2), helium separation (He/CH_4), *etc.*[6–12]

Membranes are classified into three main categories based on the type of material used, *i.e.*, organic, inorganic, and mixed matrix membranes. Organic polymeric membranes are widely used for gas separation applications due to their least cost and good ductility. But the relatively poor separation performance of polymeric membranes put the stopper on their extensive industrial use. Inorganic membranes, which are made up of metals, metal oxides, zeolites, silicates, and metal–organic frameworks (MOFs), exhibit exceptional chemical and thermal stability. However, with inorganic materials, it is very difficult to form defect-free membranes of different shapes such as cylindrical, hollow fiber, spiral, *etc.* The performance and fabrication limitations of different types of membranes can be smartly solved by incorporating organic or inorganic porous filler in a polymer matrix to form a MMM. Inorganic filler-based MMMs inherit the salient properties of organic and inorganic membranes. Good MMMs synergistically increase the

[a]Chemical Engineering Department, King Fahad University of Petroleum and Minerals, Dhahran 31261, Saudi Arabia. E-mail: alshammari@kfupm.edu.sa

[b]King Abdulaziz City for Science and Technology—Technology Innovation Centre on Carbon Capture and Sequestration (KACST-TIC on CCS) at King Fahd University of Petroleum and Minerals, Dhahran 31261, Saudi Arabia

[c]Material Discovery Research Unit, Advanced Research Center for Development, Royal Scientific Society (RSS), Amman 11941, Jordan

[d]Center of Research Excellence in Nanotechnology, King Fahd University of Petroleum and Minerals, Dhahran 31261, Saudi Arabia

permeability and/or selectivity of the polymer. The commonly used fillers in membranes are zeolites, silicates, metal oxides, carbon-based nanomaterials, and MOFs. MOFs are advanced porous materials that have been widely used in gas storage, gas separation, sensing, and catalysis applications.[13–22] MOF-fillers are considered the best choice[23] for MMM fabrication due to the following characteristics: (1) MOFs are the best crystalline porous materials that typically show very high surface area.[24–26] This high surface area helps in increasing the surface diffusion of gases in a MOF-based MMM. (2) MOFs can be designed from a wide range of metals and organic linkers to get unprecedented topologies.[27–29] There are enormous number of unique topology MOFs that can be synthesized by slightly changing the synthesis conditions or metal salt. This provides us with huge MOF filler alternatives for the fabrication of MMMs. (3) The pore aperture and surface properties (*e.g.*, gas affinity, hydrophobicity, surface polarity, *etc.*) of a MOF can be altered by introducing various functionalities using post-synthetic modification techniques.[30,31] Thus, the gas separation performance of MOF-based MMM can be further augmented by altering the properties of MOF filler. (4) A MOF's compatibility with the polymer matrix can be further enhanced by introducing desirable functionality on the MOF surface.[32–34] The partial organic nature of MOF provides the opportunity to bind functionalized-MOF to the surface of the polymer.

Historically, Paul and Kemp[35] first time formed the MMM, for the gas separation, by dispersing zeolite 5 A in a rubbery polymer. Until now, many MMMs have been reported using different fillers with glassy and rubbery polymers. For example, Reid *et al.*[36] used an MCM-41 molecular sieve to fabricate PSF MMM for gas separation application. The resulting membrane showed an increase in the permeability of gasses without compromising the selectivity of O_2/N_2 and CO_2/CH_4 pairs. The homogenous MMM of PSF and zeolite-A nanoparticle was reported by Wang *et al.*[37] for the air separation. Uniform nanoparticles created defect-free membranes with increased permeability and selectivity. Kim and Marand[38] used mesoporous MCM-48 silica in the PSF matrix and tested the loaded membranes to find the permeability of five gases (*i.e.*, He, O_2, CO_2, N_2, and CH_4). The 10% MCM-48 loaded membrane proclaimed around an 85% increase in permeabilities of all the gases. Ahn *et al.*[39] embedded nonporous fumed silica in PSF mixed matrix membrane. They found that the permeabilities of six gases increased in all the loaded MMMs of nonporous silica and were in contrast with the Maxwell model predictions. The primary issue with the use of inorganic fillers (*i.e.*, zeolites, silicates, oxide, *etc.*) was their poor compatibility with the polymer. This resulted in the formation of low loadings MMMs.[37,38] Moreover, one of the above-mentioned MMM only showed a trade-off between permeability and selectivity.[39]

Jomekian *et al.* and Pakizeh *et al.*[40,41] modified the surfaces of MCM-41 and fumed SiO_2 using dimethyldichlorosilane (DMDCS) to form polysulfone MMMs, respectively. These silanol functionalized fillers provided better dispersion in the matrix and increased the gas separation performance (*i.e.*, selectivity). Khan *et al.*[42] modified the PSF into PSF acrylate to form MMM. Moreover, they used aminopropyl-trimethoxysilane (APTMS) as a coupling agent to covalently bind zeolite-3A to

polysufone acrylate. Zeolite-3A showed an excellent molecular sieving effect for H_2/CO_2 pair because its pore size (*i.e.*, 3 Å) is between the kinetic diameter of separating gases. The kinetic diameters and 3-D space-filling models of 6 gases are shown in Fig. 1. Dorosti *et al.*[43] used ZSM-5 as filler in the polymeric blend of polysulfone and polyimide (PSF : PI = 50 : 50 wt%). The blended membrane had a slight increase in thermal stability and separation performance as compared to the pure PSF membrane. To a certain extent, the use of surface-modified inorganic fillers increased the compatibilities of the fillers with the polymers. However, this strategy added un-necessary complications in the fabrication of slightly better membranes.

In a couple of decades, many new stable MOFs have been reported and thus used in forming MMMs. Zornoza *et al.*[44] used ZIF-8, HKUST-1, and silicate-1 to form PSF MMMs. They also used combinations of MOFs and silicate-1 (*i.e.*, ZIF-8/SC-1 and HKUST-1/SC-1) in membranes.

PSF/ZIF-8 MMM showed the best performance for the mixtures which involved the separation of permeating gases based on diffusion difference between the molecules. Whereas the HKUST-1 MMM showed good separation performance for CO_2-containing mixtures due to high CO_2 adsorption of filler. Jeazet *et al.*[45] used water-stable MIL-101(Cr)/PSF MMM for O_2/N_2 separation. At 24% loading of MIL-101, the membrane increased oxygen permeability by 4 folds without changing the selectivity. Many researchers used amine-modified MOFs (*i.e.*, NH_2-MIL-101, NH_2-MIL-53, NH_2-UiO-66, *etc.*) for MMM fabrication due to their ability to reduce interfacial defects between the phases.[46–48] NH_2-UiO-66 helped in forming 50% loaded MMM which had 8 times higher CO_2 permeability than pure PSF membrane. Sarfraz and Ba-Shammakh[49–52] reported different PSF MMMs for post-combustion carbon capture in wet conditions. Among all combinations (*i.e.*, ZIF-301, ZIF-301/GO, ZIF-302/GO, and ZIF-302/CNT), ZIF-301/GO MMM unveiled 4 times increase in CO_2 permeability and 2.4 times increase in CO_2/N_2 ideal selectivity.[50] Sorribas *et al.*[53] used mesoporous silica, coated with microporous ZIF-8, in the PSF membrane to increase the compatibility between polymer and particle phase. The porous composite (meso + micro pores) filled membranes showed an increase in permeabilities without selectivity loss.
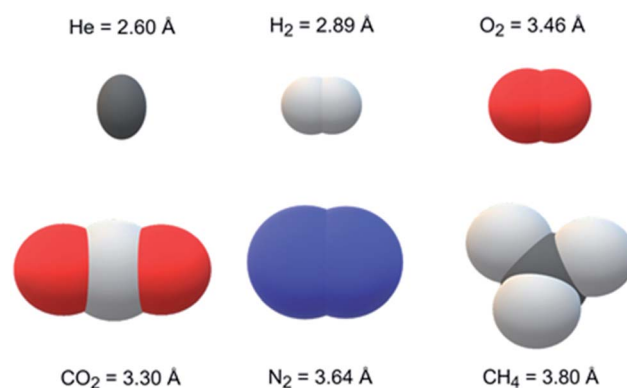

He = 2.60 Å   H₂ = 2.89 Å   O₂ = 3.46 Å

CO₂ = 3.30 Å   N₂ = 3.64 Å   CH₄ = 3.80 Å

Fig. 1 3-D space-filling models and kinetic diameters of different gases.

Jeazet *et al.*[54] simultaneously used two MOFs (*i.e.*, ZIF-8 and MIL-101) to form PSF MMMs. ZIF-8 and MIL-101(Cr) have different pore aperture (*i.e.*, 3.4 Å and 16 Å, respectively) and textural properties. The 16% loaded (ZIF-8 : MIL-101 = 1 : 1 wt) membrane showed increased perm-selectivity for CO_2/CH_4 pair. Anastasiou *et al.*[55] reported ZIF-8/graphene oxide (ZIF-8/GO) hybrid-filler MMM for separation of CO_2/CH_4 pair. The enhancement in permeability and selectivity of the membrane was attributed to the high CO_2 affinity of ZIF-8 and hindrance to diffusion of large gas molecules through GO. Cheng *et al.*[56] synthesized covalent organic framework coated (COF-coated) MOF hybrid filler for PSF MMM fabrication. They used TpPa-1 (COF) to coat the size-selective UiO-66-NH$_2$ (MOF) to increase the compatibility of filler particles. The 5% COF@MOF filler-loaded membrane increased the permeability and selectivity of CO_2 and CO_2/CH_4 by 48% and 79%, respectively. The first Bio-MOF-based PSF mixed matrix membrane was reported by Ishaq *et al.*[57] for the separation of CO_2. The membrane with 30 wt% loadings depicted a 168% increase in CO_2 permeability and a 58% increase in CO_2/N_2 selectivity. Recently, some researchers reported PSF-based membrane using carbonyl iron powder (CIP), TiO_2, and ZIF-11.[58–60] The CIP-containing PSF membranes were used for the separation of O_2 (paramagnetic) from N_2 (diamagnetic). The inclusion of magnetic powder resulted in a slight drop in separation performance, but the same membrane showed excellent performance in the presence of the unidirectionally aligned magnetic field. Under the magnetic field of 570 mT (milli Tesla), 10 wt% CIP loaded MMM revealed a 436% increase in O_2 permeability compared to a zero magnetic field environment. The researchers hypothesized that preferential magnetic channels, created by the application of magnetic field, increased the flux of paramagnetic O_2. The PSF/ZIF-11 membrane was tested for CO_2/CH_4 mixture separation.[59] The 24% PSF/ZIF-11 loaded membrane showed a 40% and 160% increase in ideal and diffusional selectivity, respectively. This increase in diffusional selectivity was achieved due to molecular sieving of gases through the narrow pore aperture of ZIF-11 (*i.e.*, 3 Å). Recently, Ilicak *et al.*[61] reported polyimide (PI) based ZIF-95 MMM for the separation of H_2 and CO_2 from natural gas. The ZIF-95 molecular sieve helped PI in improving H_2/CH_4 and CO_2/CH_4 pair selectivity by 75% and 48%, respectively. Essen *et al.*[62] reported matrimid-PBI blended (3 : 1) MMMs containing non-porous ZIF-95X and porous ZIF-301. They found that impermeable ZIF-95X/MMM does not improve the separation performance of CO_2 separation from a binary mixture of N_2 and O_2. However, the porous ZIF-301/MMM showed significant improvement in performance because its micropore volume was selectively accessible by CO_2 gas molecules.

In this work, ZIF-95 is used for the first time in PSF MMM. PSF polymer is used in membranes as a matrix due to its high tensile strength, high critical CO_2 plasticization pressure, and good chemical stability.[14] The ZIF-95 has high thermal (about 500 °C) and chemical stability.[63] The crystals of ZIF-95 exhibit POZ topology with colossal cages that have the largest pore windows of 3.65 Å (see Fig. 2). It is expected that these constricted pore windows will discriminate between the gases with different kinetic diameters. Moreover, an increase in separation

factor is anticipated for different gas pairs of H_2 and CO_2 due to the peculiar adsorption behavior of ZIF-95. The isosteric heat of adsorption of CO_2 for ZIF-95 was calculated about 24.4 kJ mol^{-1} using the Clausius–Clapeyron equation (see eqn (S1)†). POZ topology ZIF-95 have four types of cages with largest cage having 30.1×20.1 Å pore size. Such large size cages are categorized as "super cages" in zeolite-like materials. The reported BET (Langmuir) surface area (using N_2 adsorption isotherm) of ZIF-95 is 1050 m^{2}g^{-1} (1240 m^{2}g^{-1}).[63] The polar functional groups (*i.e.*, Cl) on the surface of the ZIF-95 are expected to change (*i.e.*, increase) the thermodynamic affinity (*i.e.*, solubility) of highly polarizable gases. In literature, ZIF-95 has been used in making alumina-supported membranes for the separation of H_2 and CO_2 from different gases (*i.e.*, CH_4 and N_2). Among all the reported membranes, the best selectivity was achieved in a highly oriented-ZIF-95 nano-sheet membrane.[64–66] Oriented-ZIF-95 seeding layer of 600 nm was supported on Al_2O_3 using vapor assisted in-plane epitaxial growth method. In this membrane, the permeability of hydrogen (at 1 bar and 200 °C) was around 1434.63 Barrer and the corresponding ideal selectivity of H_2/CH_4, H_2/CO_2. and CO_2/CH_4, were 64.3, 38.5, and 1.7, respectively.

2 Experimental

2.1 Materials

Zinc nitrate hexahydrate (Zn (NO$_3$)$_2$.6H$_2$O), acetone (C$_3$H$_6$O, 99%), and chloroform (CHCl$_3$, stabilized with 0.5% ethanol) were purchased from Loba Chemie Pvt. Ltd. 5-Chlorobenzimidazole (C$_7$H$_5$ClN$_2$, 96%) linker, for the synthesis of ZIF-95, was purchased from Sigma-Aldrich Co. (China). For the solvothermal synthesis of ZIF-95, dimethylformamide (DMF, 99.5%) solvent was purchased from Fisher Scientific Co. All the chemicals were used without further purification or treatment. The commercial-grade polysulfone (PSF) with average molecular weight ~35 000 and density of 1.25 g cm^{-3} (at 25 °C) was purchased from Sigma-Aldrich Co. (USA).
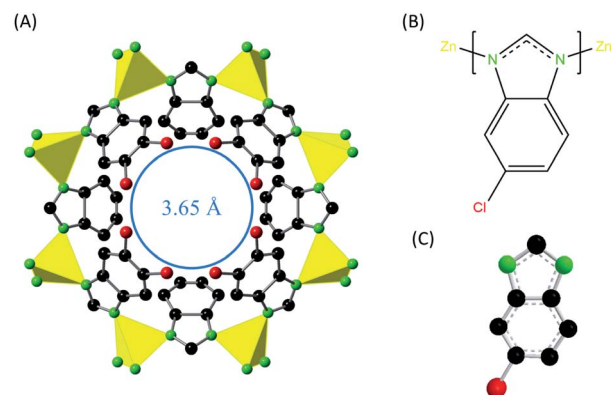

Fig. 2 (A) Structure of ZIF-95 showing largest pore window (blue circle), metal nodes (yellow pyramid), carbon atoms (black balls), nitrogen atoms (green balls), and chloride atoms (red balls). (B) Structure of 5-Cholorbenzimidaziole linker showing chlorine functional group (red) and the bonds between nitrogen atoms (green) and zinc atoms (yellow). (C) Ball and stick model of 5-Chlorobenzimidazole linker with same color scheme.

2.2   Synthesis of ZIF-95

ZIF-95 was synthesized by slight modification in the previously reported solvothermal synthesis method.[63] Zinc nitrate hexahydrate (69.5 mg, 0.234 mmol) metal salt and 5-chlorobenzimidazole (355 mg, 2.34 mmol) linker were added in Teflon lined autoclave container. Subsequently, DMF solvent (17.2 ml) was added to the same container. It is noteworthy that DMF used for the synthesis contained 0.02 percent water by weight. The container was closed tightly and placed in a gravity convection oven at 120 °C for 72 hours. The autoclave was removed from the oven on completion of 72 hours and allowed to cool down at room temperature. The ZIF-95 crystals were then washed thoroughly with DMF to remove the un-reacted materials. The yield was around 80% with respect to zinc nitrate hexahydrate. The sample was then activated (see Section S2†) for further characterizations and membrane fabrication.

2.3   Membranes fabrication

PSF beads were degassed at 100 °C for 24 hours in an oven before using them in membrane fabrication. 500 mg of PSF was dissolved in 2 ml of chloroform in a vial using a stirrer. The resulted solution of polymer was placed on stirring for 24 hours to get the homogenous solution. Afterward, degassing of the homogenous solution was done for 1 hour using sonication, and the solution was again placed under stirring for 1 more hour. The homogenous solution of polymer was cast on a clean glass plate using a casting knife. The MMMs were prepared by using two vials of 5 ml and 2 ml. The weighted quantity of PSF was dissolved in 1.4 ml of chloroform using a stirrer in a 5 ml vial. At the same time, weighted quantity ZIF-95 was added in a 2 ml vial and placed inside the vacuum oven for degassing at 110 °C for 24 hours. After 24 hours, a 2 ml vial was removed from the vacuum oven and 0.6 ml of chloroform was added to it. Sonication was used to completely disperse the ZIF-95 particle in chloroform. Subsequently, suspension of ZIF-95 was added in a 5 ml vial using a priming method to minimize the interface stress between polymer and particles.[67] Accordingly, around 20% of the suspension was added to the solution of polymer, and the resulted mixture was placed on the stirring. After 10 minutes, a further 20% of the suspension was added to the polymer solution vial. This procedure was repeated until all the suspension was added in a 5 ml vial. The remaining 0.4 ml chloroform was used to rinse a 2 ml vial and subsequently added in a 5 ml vial. Homogenous suspension of ZIF-95, PSF, and chloroform was placed under stirring for 24 hours. From then onwards, the fabrication procedure of MMM was the same as for pure polymeric membrane. The weight percent of polymer and MOF in solution was fixed to 14.37% in each membrane. All the membranes were cast on a glass plate using a doctors' knife with a gate height of 300 to 380 μm.

2.4   Characterization techniques

The crystal structure of synthesized ZIF-95 was characterized by comparing powder X-ray diffraction peaks with the simulated X-ray diffraction pattern. The PXRD data were collected by using Rigaku Miniflex-II equipment, operated at 450 watts (30 kV, 15 mA; 450 W) using Cu Kα radiation ($\lambda = 0.154$ nm). The measurement was obtained from 2–30° (2θ) with a scan rate of $1°$ min^{-1} to get good results.

The surface area of the synthesized ZIF-95 sample was calculated by using an N_2 adsorption isotherm at 77 K. Autosorb IQ equipment was used to get adsorption and desorption isotherms for ZIF-95. The CO_2 adsorption isotherm was also obtained for a sample at 273, 298, and 308 K (see Fig. S1†). The FE-SEM images of ZIF-95 crystals and membranes were obtained by using a Tescan Lyra-3 scanning electron microscope. All the samples of ZIF-95 and membranes were gold (Au) coated to increase the sample's conductivity and reduce the charging effect. Membrane samples were cryo-fractured using liquid nitrogen to see the cross-section. FE-SEM scans showed beautiful crystals of random morphology with particle sizes less than 5 μm. For a cross-section of membranes, EDS mapping was also used to see the dispersion of particles inside the cross-section of the membrane. The thicknesses of all the membranes were calculated by using SEM images.

Thermogravimetric analyses of ZIF-95 and membranes were performed using TA Q500 equipment. The dynamic high-resolution setting was selected in software to perform analysis from 30 to 770 °C. The sample was placed on a platinum pan under a dry air environment. The flow rate of dry air was maintained at 40 ml min^{-1} during analysis.

Differential scanning calorimetry was also used to find the glass transition temperature (T_g) of pure and loaded membranes. A slight increase in T_g was observed for MMM as loading increased.

2.5   Permeation measurement

The membranes permeation performance was measured for 6 gasses, i.e. He, H_2, O_2, CO_2, N_2, and CH_4. Constant volume/variable pressure (CV/VP) permeation setup (see Fig. S2†) was used to calculate the permeability of each gas. The feed side and permeate side of the permeation setup were evacuated to 35 mTorr pressure before each measurement. The temperature of setup was maintained at 35 °C and feed side pressure was raised to 1550 torr to start each run. The change in pressure with respect to time was used to calculate the flux of the gas through the membrane using eqn (S3).† This flux was then used to calculate the permeability coefficient or permeability of the gases. Permeability coefficient (P_i) is defined as follow:

$$P_i = \frac{\text{Flux}_i L}{\Delta p}$$

$$1 \text{ Barrer} = 10^{-10} \text{ cm}^3 \text{ (STP) cm cm}^{-2} \text{ s}^{-1} \text{ cmHg}^{-1}$$

where "P_i" is the permeability of gas "i", "L" is the thickness of the membrane, and "Δp" is the pressure difference between upstream and downstream of membrane.

The ideal selectivity (S_{ij}) is expressed as follow:

$$S_{ij} = \frac{P_i}{P_j} \quad \text{unit less quantity}$$

where "P_i" and "P_j" is the permeability of gas "i" and "j", respectively.
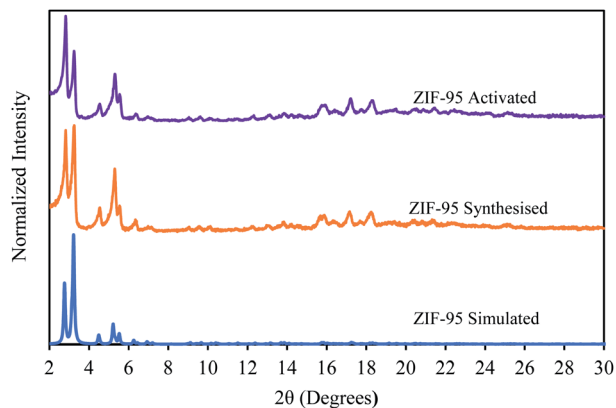
Fig. 3 Powder X-ray diffraction pattern of simulated (blue), synthesized (orange), and activated (purple) ZIF-95.

Fig. 5 SEM images of a cross-section of 8% loaded membrane (A, a) and 16% loaded membrane (B, b).

Since the results of mostly reported MMMs are at different temperature and pressure conditions so we cannot depict performance increase by just permeability and selectivity. Moreover, the literature also reports symmetric and asymmetric membranes that show completely different permeability and selectivity. So, we have calculated a percentage performance increase for MMMs as compared to the pure membranes.

3 Results and discussion

3.1 Characterizations

The powder X-ray diffraction pattern (see Fig. 3) of the synthesized ZIF-95 exhibits characteristic diffraction peaks at 2.83, 3.22, and 5.30. These peaks match exactly with the simulated diffraction pattern obtained from the crystallographic information file (CIF) using Mercury software. The slight increase in intensities of the first diffraction peak appeared immediately after the activation of the ZIF-95 sample. A similar trend was seen in the earlier study.[68] Overall, there was no change in the crystallinity after activation of the sample.

In Fig. 4, the SEM images of ZIF-95 and pure PSF membrane are presented. As shown in Fig. 4(A, a), the average particle size
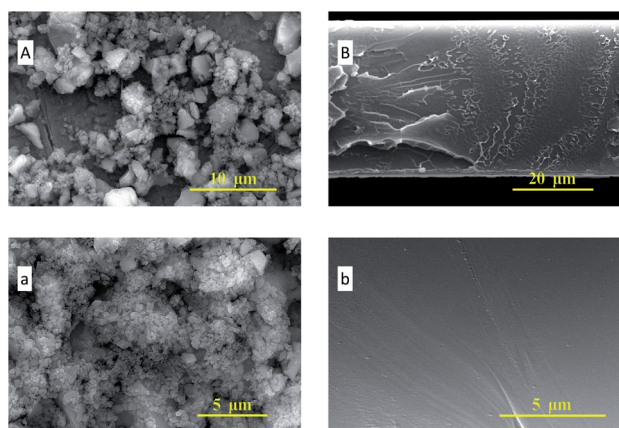
of synthesized ZIF-95 was less than 5 μm. The SEM images of the pure membrane (i.e., Fig. 4(B, b)) show symmetric dense structure. The thickness of each membrane was measured using SEM images of the cross-section. The SEM images of loaded MMMs (see Fig. 5 and 6) showed good adhesion between particles and the polymer. The non-uniform-sized particles were distributed evenly in the polymer matrix. Fig. 5(A, a) and (B, b) show that the particles of ZIF-95 were distributed uniformly in 8% and 16% loaded membranes, respectively, but there was a huge distance in the position of adjacent particles. However, in 24% and 32% loaded membranes (see Fig. 6(A, a) and (B, b), respectively) the particles were present closer to each other. This closeness in position particles might have formed porous channels of ZIF-95 inside the polymer matrix.

The distribution of ZIF-95 particles inside loaded membranes was also seen through electron dispersion spectroscopy (EDS) mapping using a constant scanning rate. The zinc was selected as a mapping element in EDS scans (Fig. S3†). EDS scans also revealed that the particles were distributed uniformly inside all the membranes.

The N_2 adsorption isotherm (at 77 K) was used to calculate the porosities and surface area of synthesized ZIF-95 samples

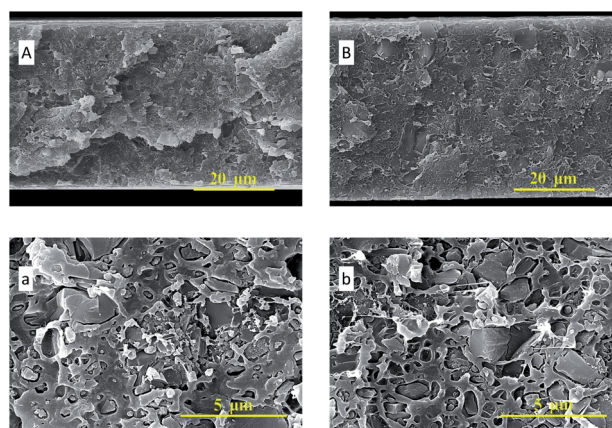Fig. 4 SEM images of ZIF-95 (A, a) and cross-section of a pure membrane (B, b).

Fig. 6 SEM images of the cross-section of 24% loaded membrane (A, a) and 32% loaded membrane (B, b).
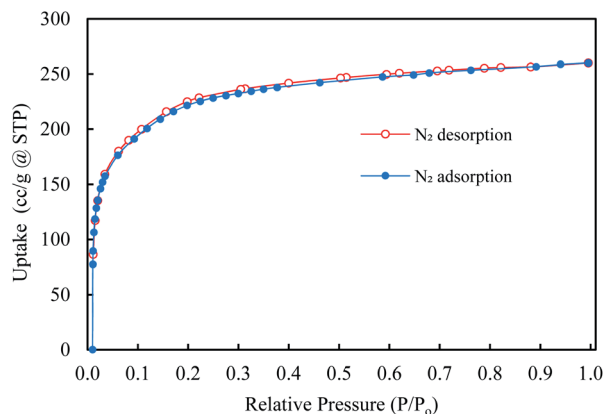
Fig. 7 Nitrogen adsorption (blue) and desorption (red) isotherm at 77 K for ZIF-95.

Table 1 Glass transition temperature (T_g) of pure and loaded membranes

Membranes	Glass transition temperature (T_g) (°C)
Pure PSF	185.02
PSF-ZIF-95–8%	185.09
PSF-ZIF-95–16%	185.28
PSF-ZIF-95–24%	185.40
PSF-ZIF-95–32%	185.96

(see Fig. 7). Brunauer–Emmett–Teller (BET) and Langmuir surface areas were calculated using adsorption points from 0.03–0.08 and 0.1–0.35, respectively. Accordingly, the BET (Langmuir) surface area synthesized MOF was found to be 850 $\pm$ 50 (1100 $\pm$ 50) m^2 g^{-1}. Moreover, the total micropore pore volume was around 0.41 cm^3 g^{-1}. The CO_2 adsorption isotherms were obtained at 273 K, 298 K, and 308 K (see Section S1, Fig. S1†). The isosteric heat of CO_2 adsorption (Q_{st}) for ZIF-95 was calculated using the Clausius–Clapeyron equation. The Q_{st} value of ZIF-95 was around 24.4 kJ mol^{-1}, which confirms that the adsorption of CO_2 is physisorption in nature.

The thermogravimetric analysis (TGA) of activated ZIF-95 and membranes were done in a dry air environment (Fig. 8). The thermal stability of ZIF-95 was around 400 °C in air, slightly less than stability reported in only N_2 ($\sim$500 °C) environment.[63] The residual weight of ZIF-95 was about 19.08 grams per 100 grams of ZIF-95. This is in complete agreement with the theoretical calculations of a completely oxidized metal framework. The theoretical residual weight of the oxidized framework (ZnO) was calculated to be 20 g per 100 g of ZIF-95. The slight difference in theoretical and actual residual weight may arise due to adsorbed solvent/gases and/or instrument calibration.

The weight of residue was also used to verify the loadings of MMM. For pure membrane, the residue's weight was close to zero (*i.e.* 0.29%) due to the complete burning of PSF into oxide gases (*i.e.*, CO_2, H_2O, SO_2, *etc.*). The residual weight of each loaded membrane was in accordance with the loading of the corresponding MMM. The residual weights for 8%, 16%, 24%, and 32% loaded membranes were about 1.92%, 3.12%, 4.65%, and 6.27%, respectively.

Differential scanning calorimetry of all the membrane samples was done to check the glass transition temperature (T_g). The glass transition temperature of membranes increased slightly as the loading of filler increased (see Table 1). Since the increase in T_g is not very pronounced, so it cannot be used to indicate interfacial interaction between particles and polymer chains. An increase in T_g is often related to the rigidification of polymer chains. Usually, Chain rigidification limits the movement of chains and consequently increases the selectivity of the membrane. The DSC thermograms of pure and loaded membranes are provided in Section S5.†

3.2 Gas permeation and selectivity of MMM

The pure PSF membrane and MMMs were tested for the permeability of six gases. Among these gases, CO_2 and CH_4 usually have greater interaction with the PSF matrix than He, H_2, O_2, and N_2. The more interacting gases (*i.e.*, CO_2 and CH_4) have greater condensability and polarizability.[69] Primarily all the considered gases are non-polar, but they have different polarizability. The polarizabilities of He, H_2, O_2, N_2, CH_4, and CO_2 are 2×10^{-25} cm^3, 8.2×10^{-25} cm^3, 15.8×10^{-25} cm^3, 17.6×10^{-25} cm^3, 26.0×10^{-25} cm^3, and 26.3×10^{-25} cm^3,
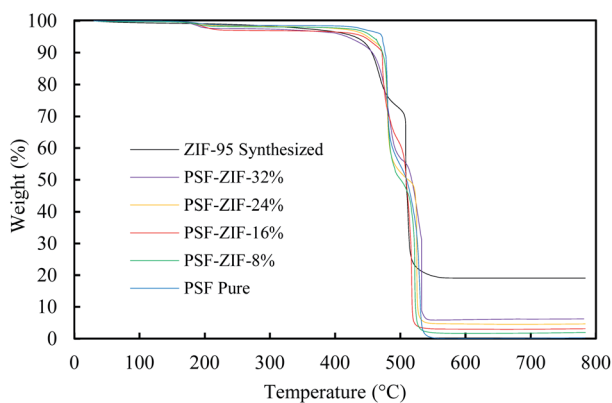

Fig. 8 Thermogravimetric analysis of ZIF-95 (black), pure membrane (blue), and 8% loaded membrane (green), 16% loaded membrane (red), 24% loaded membrane (orange), and 32% loaded membrane (purple).
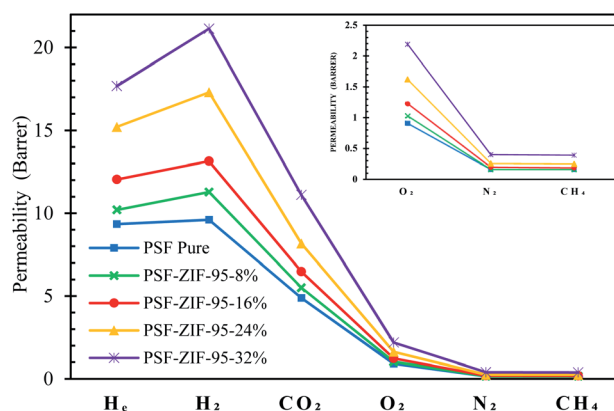

Fig. 9 Permeability of six gases through pure and loaded mixed matrix membranes.

respectively.[70,71] Fig. 9 shows the permeability of all the gases through membranes in the scatter plot. In general, each membrane followed decreasing trend of permeability such that $P_{H_2} > P_{He} > P_{CO_2} > P_{O_2} > P_{N_2} \geqq P_{CH_4}$. All the membranes showed P_{H_2} more than P_{He} even though the size of helium is less than hydrogen. This divergence in permeability is because helium is an inert gas and has very low polarizability and condensability. Briefly, polysulfone polymer doesn't interact much with helium due to its low condensability and low polarizability. The ideal selectivity of 13 gas pairs are calculated in ESI, Section S6 (Table S2†). Since all the synthesized membranes were dense, that is why they showed very high selectivity for different gases separation. The permeabilities and selectivity of already reported MMMs are tabulated in Section S8 of ESI (Tables S5–S8†).

Compared to the pure membrane, an increase in permeabilities was observed as the loading of ZIF-95 was increased in the MMMs. The permeation increases in the 8%, 16%, and 24% loaded membranes were achieved without any loss in the selectivity of nearly all the separation pairs. The maximum increase in permeability of gases was observed in the 32% loaded membrane. However, this increase in permeability did not improve the overall gas separation performance extraordinarily, because the selectivity of this membrane slightly decreased at this high loading. The high loading might have formed nonselective voids in the 32% loaded membrane, which usually result in the decrease of selectivity. In an 8% loaded membrane, the permeability of He, H₂, O₂, and CO₂ increased by 9.2%, 17.5%, 13.2%, and 12.7%, respectively.

The permeability of methane and nitrogen did not increase at all in the least loaded membrane. Consequently, this least loaded membrane showed a maximum increase in selectivity of almost all the separation pairs involving large kinetic diameter gases (*i.e.*, N₂ and CH₄). The selectivity of H₂/CH₄ or H₂/N₂, CO₂/CH₄ or CO₂/N₂, He/CH₄ or He/N₂, O₂/N₂, H₂/CO₂, and H₂/O₂ pairs increased by about 17.5%, 12.7%, 9.2%, 13.2%, 4.3%, and 3.8%, respectively, when compared to the pure PSF membrane. The 16% loaded membrane showed a permeability increase for all the gases, *i.e.*, 28.9%, 36.9%, 35.2%, 32.6%, 21.9%, and 16.3% in He, H₂, O₂, N₂, CH₄, and CO₂, respectively. The selectivity of this membrane was almost similar to that of previous membrane. The 24% loaded membrane produced the maximum permeability increase without compromising selectivity. Hence, 24% loaded membrane is considered as optimal performance membrane with optimal loading. Optimal loading of MOF in a polymer depends on many factors such as particle size, the interaction of MOF with polymer, fabrication procedure, partials distribution in a membrane, filler density, *etc.* In 24% loaded membrane, the permeability of He, H₂, O₂, CO₂, N₂, and CH₄ increased by 62.8%, 80.2%, 78.0%, 67.2%, 60%, and 56.3%, respectively. Fig. 9 shows a sharp increase in permeability of gases in 24% percent loaded membranes, as compared to other membranes. This sharp increase could be due to the formation of porous channels of the ZIF-95 sieve in the polymer matrix. At low loading, these channels are usually not present due to the huge difference between positions of particles in the polymer matrix. The porous channels are sometimes formed at very high weight percent loading in MMM due to the high

difference in density of the filler and polymer matrix. In 24% loaded membrane, the selectivity of H₂/CH₄, H₂/N₂, H₂/CO₂, O₂/N₂, CO₂/CH₄, CO₂/N₂, He/CH₄, and N₂/CH₄ pairs increased by about 15.6%, 12.6%, 7.8%, 10.8%, 6.9%, 4.6%, 4.2%, and 2.4%, respectively, as compared to the pure PSF membrane.

3.3 Gas transport mechanism

The transport properties of gases through the pure and loaded MMMs were also studied by using the solution diffusion model.[71] This model is commonly used to understand the kinetic transport behavior and interaction of gas molecules within the polymer. MMM containing porous fillers are the best membranes for applying the solution diffusion model (*i.e.*, $P = D \times S$). The model defines permeability (P) as a product of solubility coefficient (S) and diffusivity coefficient (D). Whereas diffusivity coefficient can be calculated using time lag (θ) correlation (given below). Time lag (θ) is defined as the *x*-intersect of the steady-state line in the time *vs.* flux graph of permeation measurement. The simple division of calculated permeability with diffusivity coefficient gives us the value of solubility coefficient.

$$D = l^2/6\theta$$

where, "l" is the thickness of membrane in cm and "θ" is the time lag in seconds.

The calculated values of solubility coefficients and diffusivity coefficients of mixed matrix membranes are given in ESI (Section S7†). For further elaboration, the diffusivity coefficient and solubility coefficient are correlated to the kinetic diameter and normal boiling point of gases, respectively (see Fig. 10 and 11). The diffusivity coefficient reflects the kinetic transport behavior of gases through the membrane pores and the solubility coefficient reflects the thermodynamic interaction of gases with the membrane.[13]

The inclusion of ZIF-95 in the PSF increased the diffusivity of almost all the gases as the loading increased. The increase in diffusivity was not uniform for all the gases, rather there was more increase in diffusivities of small kinetic diameter gases.
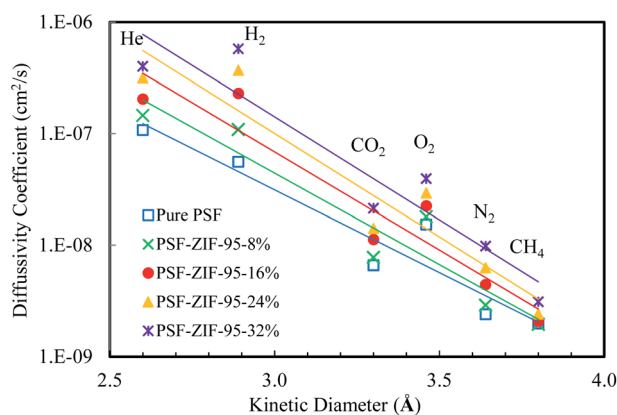

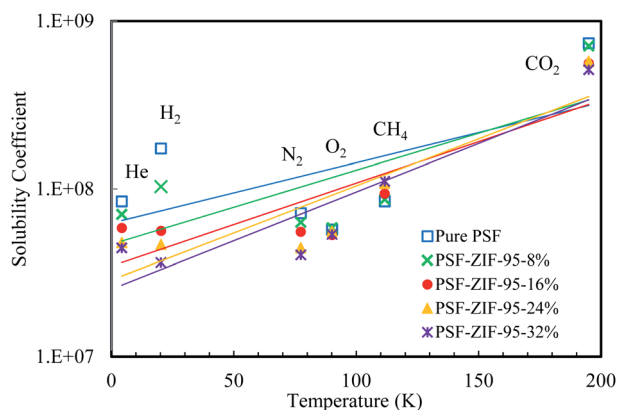**Fig. 10** Diffusivity coefficient (cm² s⁻¹) *vs.* kinetic diameter (Å) plot of pure and loaded mixed matrix membranes.

Fig. 11 Solubility coefficient [cm^3 (gas) cm^{-3} (ZIF) cmHg] *vs.* boiling point (K) plot of pure and loaded mixed matrix membranes.

The most significant increase was observed in the diffusivity coefficient of hydrogen gas in the loaded membranes. The increased hydrogen gas separation performance of loaded membranes is due to the fast diffusion of hydrogen gas molecules through ZIF-95 pores. In optimal loaded membrane (*i.e.*, 24%), the hydrogen gas diffusivity increased by almost 6.6 times (*i.e.*, 560% increase) of the pure membrane. The least increase was observed in the diffusivity of methane gas (*i.e.*, 1.5 times) due to its largest kinetic diameter. The other gases, such as, He, O_2, CO_2, and N_2 showed 194.1%, 91.6%, 114.0%, and 161.7% increase in diffusivity as compared to the pure membrane, respectively.

The incorporation of ZIF-95 in PSF decreased the solubility of all gases (except methane), as the loading increased. For low boiling point gases (*i.e.*, He and H_2), a sharp decrease in solubility was observed as the loading increased. In 24% loaded membrane, the minimum decrease was observed in the solubility of O_2 and CO_2 (*i.e.*, 5.8% and 40.2%, respectively). The slight decrease in solubilities did not decrease the overall permeability of both gases in the optimal loaded membrane. So, the increase in separation performance of some O_2 and CO_2 gas pairs can be attributed to the sharp decrease in solubilities of other gases. The solubility of hydrogen decreased 3.7 times (*i.e.*, −72.3% decrease) and the solubility of methane increased 1.3 times (*i.e.*, 28.3% increase) of the pure membrane in the optimal loaded membrane. The only gas which showed an increase in solubility with an increase in loading of ZIF-95 was methane. But the effect of increased solubility on methane permeability was minimized due to its very low diffusivity. The solubility of He and N_2 decreased by −44.7% and −37.9%, respectively, when compared to the pure membrane. The upper bound plots for 13 gas pairs are given in ESI (see Fig. S5 to S17), Section S9,† to visualize the performance increase in all the synthesized membranes.

The diffusivity and solubility selectivity of different gas pairs are reported in Tables S3 and S4,† respectively. The diffusivity selectivity of helium gas pairs (*i.e.*, He/O_2, He/CO_2, He/N_2, and He/CH_4) increased as the loading of ZIF-95 was increased until the optimal loading was reached (except for He/H_2). The

optimal loaded membrane showed the selectivity increase of 141.8%, 53.5%, 37.4%, and 12.3% for He/CH_4, He/O_2, He/CO_2, and He/N_2 pairs, respectively. In 32% loading membrane, the diffusivity selectivity of the He gas pairs were slightly less than the optimal loading membrane. The diffusion selectivity of all the hydrogen gas pairs (*i.e.*, H_2/O_2, H_2/CO_2, H_2/N_2, and H_2/CH_4) increased as the loading of ZIF-95 increased in each successive membrane. The optimal loaded membrane showed the diffusion selectivity increase of 443.2%, 244.9%, 208.7%, and 152.5% for H_2/CH_4, H_2/O_2, H_2/CO_2, and H_2/N_2 pairs, respectively. The CO_2/CH_4 and N_2/CH_4 pairs displayed an increase in selectivity as the loading of filler was increased in the membranes. Conversely, the CO_2/N_2 and O_2/N_2 pairs showed selectivity decrease as the loading was increased in the PSF membranes. Compared to a pure membrane, the optimal loaded membrane depicted an increase/decrease of 115.2%, 76.0%, −18.2%, and −26.8% for N_2/CH_4, CO_2/CH_4, CO_2/N_2, and O_2/N_2 pairs, respectively.

The solubility selectivity of helium gas pairs (*i.e.*, He/O_2, He/CO_2, He/N_2, and He/CH_4) decreased as the loading of ZIF-95 was increased in the PSF. This trend in solubility selectivity is obvious due to the low polarizability and condensability of He when compared to CO_2, CH_4, N_2, and O_2. Interestingly the He/H_2 pair showed an increase in the solubility selectivity as loading was increased in the polymer. This could be explained by considering the inverse relation in the solubility and diffusivity (*i.e.*, $P = D \times S$). The fast-diffusing H_2 gas molecules don't interact much with the membrane and decrease the solubility which causes the increase in He/H_2 solubility selectivity. The solubility selectivity of hydrogen gas pairs (*i.e.*, H_2/O_2, H_2/CO_2, H_2/N_2, and H_2/CH_4) decreased as the loading of filler was increased in the membranes. This solubility selectivity decrease in the above-mentioned gas pairs is due to the fact that all other gases have more polarizability and condensability than hydrogen gas. The CO_2/N_2 and O_2/N_2 pairs showed an increase in solubility selectivity as the loading of ZIF-95 was increased in the membranes. In fact, the CO_2 gas has more polarizability than N_2 gas and O_2 gas has more condensability than N_2 gas. This analogy in polarizability and compatibility may have played its role in increasing the solubility selectivity of CO_2/N_2 and O_2/N_2 pairs. The remaining 2 pairs of methane gas (*i.e.*, CO_2/CH_4 and N_2/CH_4) showed a decrease in solubility selectivity as we moved towards high loading membranes. In optimal loaded membrane the solubility selectivity decreased/increased by −79.1%, −72.5%, −65.7%, −56.9%, −56.8%, −51.6%, −43.4%, −39.0%, −29.3%, −11.0%, 25.9%, 57.3%, and 105.9% for H_2/CH_4, H_2/O_2, H_2/CO_2, He/CH_4, H_2/N_2, N_2/CH_4, He/O_2, CO_2/CH_4, He/CO_2, He/N_2, CO_2/N_2, O_2/N_2, and He/H_2 pairs, respectively.

4 Conclusions

The novel ZIF-95/PSF mixed matrix membranes showed an increase in permeabilities of all the considered gasses as the loading of ZIF-95 was increased in PSF. The increase in permeability was not uniform for each gas because the diffusivities and solubilities of the gases were changed differently in

the MMMs. However, the small kinetic diameter gases passed through the molecular sieve (*i.e.*, ZIF-95) quite easily. And the large kinetic diameter gases faced the hindrance in diffusional flow. Overall, the compatibility between ZIF-95 and PSF was very good. Among all the gases, the best separation performance was observed for the hydrogen gas separation. In an optimal loaded membrane, the permeability of hydrogen increased by 80.2% as compared to the pure membrane. Moreover, the selectivity of H_2/CH_4 and H_2/N_2 increased by 15.3% and 12.6% when compared with pure polysulfone membrane, respectively. The DSC analysis confirms that the increase in selectivity is not due to polymer chain rigidification. Instead, it is due to the molecular sieving of large kinetic diameter gas (*i.e.*, CH_4). Membranes of ZIF-95/PSF have considerably increased the separation of H_2/N_2 and H_2/CH_4 gas pairs. The slight decrease in the selectivity of 32% loaded membrane could be due to the agglomeration of micro-sized particles.

Author's contributions

Sanaullah Shafiq: conceptualization, writing original draft, data collection, methodology. Bassem A. Al-Maythalony: methodology, resources, review & editing, formal analysis. Muhammad Usman: Data Curation, Software, Visualization, Review. Mohammad Saleh Ba-Shammakh: Formal analysis, Interpretation of data. Abdallah A. Al-Shammari: Supervision, Review & editing, Investigation, validation.

Conflicts of interest

There are no conflicts to declare.

Acknowledgements

References

1 R. W. Baker, *Membrane technology and applications*, John Wiley & Sons, 2012.

2 M. D. Garba, M. Usman, M. A. J. Mazumder, A. Al-Ahmed and Inamuddin, *Environ. Chem. Lett.*, 2019, **17**, 1195–1208.

3 M. Sarfraz, in *Membranes for Environmental Applications*, 2020, Carbon capture via mixed-matrix membranes containing nanomaterials and metal-organic frameworks, vol. 42, p. 45.

4 B. A. Al-Maythalony, in *Advanced Nanomaterials for Membrane Synthesis and its Applications*, Elsevier, 2019, Metal-organic framework based membranes for gas separation, pp. 203–226.

5 R. Ben-Mansour, M. A. Habib, O. E. Bamidele, M. Basha, N. A. A. Qasem, A. Peedikakkal, T. Laoui and M. Ali, *Appl. Energy*, 2016, **161**, 225–255.

6 J. Wilcox, *Carbon capture*, Springer Science & Business Media, 2012.

7 M. G. Buonomenna, *RSC Adv.*, 2013, **3**, 5694–5740.

8 C. A. Scholes and U. K. Ghosh, *Membranes*, 2017, **7**, 9.

9 B. Chen, Z. Yang, Y. Zhu and Y. Xia, *J. Mater. Chem. A*, 2014, **2**, 16811–16831.

10 V. V. Belousov, S. V. Fedorov and M. S. J. J. o. t. E. S. Sedov, *J. Electrochem. Soc.*, 2019, **166**, H573.

11 K. Xie, Q. Fu, G. G. Qiao and P. A. Webley, *J. Membr. Sci.*, 2019, **572**, 38–60.

12 C. Li, J. J. Chew, A. Mahmoud, S. Liu and J. Sunarso, *J. Membr. Sci.*, 2018, **567**, 228–260.

13 A. S. Ghanem, M. Ba-Shammakh, M. Usman, M. F. Khan, H. Dafallah, M. A. M. Habib and B. A. Al-Maythalony, *J. Appl. Polym. Sci.*, 2020, **137**, 48513.

14 M. A. Jafar Mazumder, P. H. Raja, A. M. Isloor, M. Usman, S. H. Chowdhury, S. A. Ali, Inamuddin and A. Al-Ahmed, *Sci. Rep.*, 2020, **10**, 7049.

15 M. D. Garba, M. Usman, S. Khan, F. Shehzad, A. Galadima, M. F. Ehsan, A. S. Ghanem and M. Humayun, *J. Environ. Chem. Eng.*, 2021, **9**, 104756.

16 A. Helal, K. E. Cordova, M. E. Arafat, M. Usman and Z. H. Yamani, *Inorg. Chem. Front.*, 2020, **7**, 3571–3577.

17 L. E. Kreno, K. Leong, O. K. Farha, M. Allendorf, R. P. Van Duyne and J. T. Hupp, *Chem. Rev.*, 2012, **112**, 1105–1125.

18 K. Tan, S. Zuluaga, E. Fuentes, E. C. Mattson, J.-F. Veyan, H. Wang, J. Li, T. Thonhauser and Y. J. Chabal, *Nat. Commun.*, 2016, **7**, 13871.

19 A. Helal, M. Usman, M. E. Arafat and M. M. Abdelnaby, *J. Ind. Eng. Chem.*, 2020, **89**, 104–110.

20 L. Yang, Y.-L. Liu, C.-G. Liu, Y. Fu and F. Ye, *RSC Adv.*, 2020, **10**, 19149–19156.

21 B.-B. Lu, X. Han, C.-J. Feng, D. Wang and F. Ye, *Crystals*, 2021, **11**, 574.

22 L. Yang, Y.-L. Liu, C.-G. Liu, F. Ye and Y. Fu, *J. Hazard. Mater.*, 2020, **381**, 120966.

23 Y. Zhang, X. Feng, S. Yuan, J. Zhou and B. Wang, *Inorg. Chem. Front.*, 2016, **3**, 896–909.

24 H. K. Chae, D. Y. Siberio-Pérez, J. Kim, Y. Go, M. Eddaoudi, A. J. Matzger, M. O'Keeffe, O. M. Yaghi, D. Materials and G. Discovery, *Nature*, 2004, **427**, 523–527.

25 O. K. Farha, A. Özgür Yazaydın, I. Eryazici, C. D. Malliakas, B. G. Hauser, M. G. Kanatzidis, S. T. Nguyen, R. Q. Snurr and J. T. Hupp, *Nat. Chem.*, 2010, **2**, 944–948.

26 S.-i. Noro, D. Tanaka, H. Sakamoto, S. Shimomura, S. Kitagawa, S. Takeda, K. Uemura, H. Kita, T. Akutagawa and T. Nakamura, *Chem. Mater.*, 2009, **21**, 3346–3355.

27 R. Banerjee, A. Phan, B. Wang, C. Knobler, H. Furukawa, M. O'Keeffe and O. M. Yaghi, *Science*, 2008, **319**, 939–943.

28 O. K. Farha and J. T. Hupp, *Acc. Chem. Res.*, 2010, **43**, 1166–1175.

29 J. Yang, Y.-B. Zhang, Q. Liu, C. A. Trickett, E. Gutiérrez-Puebla, M. Á. Monge, H. Cong, A. Aldossary, H. Deng and O. M. Yaghi, *J. Am. Chem. Soc.*, 2017, **139**, 6448–6455.

30 B. A. Al-Maythalony, A. M. Alloush, M. Faizan, H. Dafallah, M. A. A. Elgzoly, A. A. A. Seliman, A. Al-Ahmed, Z. H. Yamani, M. A. M. Habib, K. E. Cordova and O. M. Yaghi, *ACS Appl. Mater. Interfaces*, 2017, **9**, 33401–33407.

31 T. Islamoglu, S. Goswami, Z. Li, A. J. Howarth, O. K. Farha and J. T. Hupp, *Acc. Chem. Res.*, 2017, **50**, 805–813.

32 X. Jiang, S. Li, S. He, Y. Bai and L. Shao, *J. Mater. Chem. A*, 2018, **6**, 15064–15073.

33 L. Maserati, S. M. Meckler, J. E. Bachman, J. R. Long and B. A. Helms, *Nano Lett.*, 2017, **17**, 6828–6832.

34 M. Usman, M. Ali, B. A. Al-Maythalony, A. S. Ghanem, O. W. Saadi, M. Ali, M. A. Jafar Mazumder, S. Abdel-Azeim, M. A. Habib, Z. H. Yamani and W. Ensinger, *ACS Appl. Mater. Interfaces*, 2020, **12**, 49992–50001.

35 D. R. Paul and D. R. Kemp, *J. Polym. Sci.*, 1973, **41**, 79–93.

36 B. D. Reid, F. A. Ruiz-Trevino, I. H. Musselman, K. J. Balkus and J. P. Ferraris, *Chem. Mater.*, 2001, **13**, 2366–2373.

37 H. Wang, B. A. Holmberg and Y. Yan, *J. Mater. Chem.*, 2002, **12**, 3640–3643.

38 S. Kim, E. Marand, J. Ida and V. V. Guliants, *Chem. Mater.*, 2006, **18**, 1149–1155.

39 J. Ahn, W.-J. Chung, I. Pinnau and M. D. Guiver, *J. Membr. Sci.*, 2008, **314**, 123–133.

40 A. Jomekian, M. Pakizeh, A. R. Shafiee and S. A. A. Mansoori, *Sep. Purif. Technol.*, 2011, **80**, 556–565.

41 M. Pakizeh, A. N. Moghadam, M. R. Omidkhah and M. Namvar-Mahboub, *Korean J. Chem. Eng.*, 2013, **30**, 751–760.

42 A. L. Khan, A. Cano-Odena, B. Gutiérrez, C. Minguillón and I. F. J. Vankelecom, *J. Membr. Sci.*, 2010, **350**, 340–346.

43 F. Dorosti, M. R. Omidkhah, M. Z. Pedram and F. Moghadam, *Chem. Eng. J.*, 2011, **171**, 1469–1476.

44 B. Zornoza, B. Seoane, J. M. Zamaro, C. Téllez and J. Coronas, *ChemPhysChem*, 2011, **12**, 2781–2785.

45 H. B. T. Jeazet, C. Staudt and C. Janiak, *Chem. Commun.*, 2012, **48**, 2140–2142.

46 B. Zornoza, A. Martinez-Joaristi, P. Serra-Crespo, C. Tellez, J. Coronas, J. Gascon and F. Kapteijn, *Chem. Commun.*, 2011, **47**, 9522–9524.

47 T. Rodenas, M. van Dalen, P. Serra-Crespo, F. Kapteijn and J. Gascon, *Microporous Mesoporous Mater.*, 2014, **192**, 35–42.

48 N. C. Su, D. T. Sun, C. M. Beavers, D. K. Britt, W. L. Queen and J. J. Urban, *Energy Environ. Sci.*, 2016, **9**, 922–931.

49 M. Sarfraz and M. Ba-Shammakh, *J. Ind. Eng. Chem.*, 2016, **36**, 154–162.

50 M. Sarfraz and M. Ba-Shammakh, *J. Membr. Sci.*, 2016, **514**, 35–43.

51 M. Sarfraz and M. Ba-Shammakh, *Arabian J. Sci. Eng.*, 2016, **41**, 2573–2582.

52 M. Sarfraz and M. Ba-Shammakh, *J. Taiwan Inst. Chem. Eng.*, 2016, **65**, 427–436.

53 S. Sorribas, B. Zornoza, C. Téllez and J. Coronas, *J. Membr. Sci.*, 2014, **452**, 184–192.

54 H. B. Tanh Jeazet, S. Sorribas, J. M. Román-Marín, B. Zornoza, C. Téllez, J. Coronas and C. Janiak, *Eur. J. Inorg. Chem.*, 2016, **2016**, 4363–4367.

55 S. Anastasiou, N. Bhoria, J. Pokhrel, K. S. Kumar Reddy, C. Srinivasakannan, K. Wang and G. N. Karanikolos, *Mater. Chem. Phys.*, 2018, **212**, 513–522.

56 Y. Cheng, Y. Ying, L. Zhai, G. Liu, J. Dong, Y. Wang, M. P. Christopher, S. Long, Y. Wang and D. Zhao, *J. Membr. Sci.*, 2019, **573**, 97–106.

57 S. Ishaq, R. Tamime, M. R. Bilad and A. L. Khan, *Sep. Purif. Technol.*, 2019, **210**, 442–451.

58 F. H. Azhar, Z. Harun, S. S. Alias, M. Z. Yunos, S. A. Ibrahim, T. Abdullahi, A. Ahmad and M. H. D. Othman, *Macromol. Res.*, 2020, **28**, 625–635.

59 A. Guo, Y. Ban, K. Yang, Y. Zhou, N. Cao, M. Zhao and W. Yang, *J. Membr. Sci.*, 2020, **601**, 117880.

60 S. Raveshiyan, S. S. Hosseini and J. Karimi-Sabet, *Chem. Eng. Process.*, 2020, **150**, 107866.

61 I. Ilicak, M. S. Boroglu, A. Durmus and I. Boz, *J. Nat. Gas Sci. Eng.*, 2021, **91**, 103941.

62 M. van Essen, R. Thür, M. Houben, I. F. J. Vankelecom, Z. Borneman and K. Nijmeijer, *J. Membr. Sci.*, 2021, **635**, 119517.

63 B. Wang, A. P. Côté, H. Furukawa, M. O'Keeffe and O. M. Yaghi, *Nature*, 2008, **453**, 207–211.

64 A. Huang, Y. Chen, N. Wang, Z. Hu, J. Jiang and J. Caro, *Chem. Commun.*, 2012, **48**, 10981–10983.

65 X. Ma, Z. Wan, Y. Li, X. He, J. Caro and A. Huang, *Angew. Chem.*, 2020, **59**, 20858–20862.

66 X. Ma, Y. Li and A. Huang, *J. Membr. Sci.*, 2020, **597**, 117629.

67 R. Mahajan and W. J. Koros, *Ind. Eng. Chem. Res.*, 2000, **39**, 2692–2696.

68 J. H. Aldrich, S. M. Rousselo, M. L. Yang, S. M. Araiza and F. Tian, *Energy Fuels*, 2019, **33**, 348–355.

69 S. Y. Sawant, R. S. Somani, H. C. Bajaj and S. S. Sharma, *J. Hazard. Mater.*, 2012, **227–228**, 317–326.

70 Z. Zhang, Z. Li and J. Li, *Langmuir*, 2012, **28**, 12122–12133.

71 B. Freeman, Y. Yampolskii and I. Pinnau, *Materials science of membranes for gas and vapor separation*, John Wiley & Sons, 2006.